Journal of Orthopaedic Translation 52 (2025) 478–491

Contents lists available at ScienceDirect

Journal of Orthopaedic Translation

journal homepage: www.journals.elsevier.com/journal-of-orthopaedic-translation

Original article

Recapitulation of *in vivo* angiogenesis and osteogenesis within an *ex vivo* muscle pouch-based coral-derived macroporous construct organoid model

Jia-run Bai [a,1], Chao Zhang [a,1], Gen Li [b,1], Yu-gang Wang [a], Yu-qi Dong [a], Roland M. Klar [c,*], Tao He [a,**]

[a] Department of Orthopedics, Renji Hospital, School of Medicine, Shanghai Jiao Tong University, Shanghai, China
[b] Department of Orthopedics, Ruijin Hospital, Shanghai Jiao Tong University School of Medicine, Shanghai, China
[c] School of Clinical Medicine - Internal Medicine, Faculty of Health Sciences, University of the Witwatersrand, Johannesburg, South Africa

ARTICLE INFO

Keywords:
Angiogenesis
Osteogenesis
Coral-derived construct
Muscle pouch-based
Organoids

ABSTRACT

Background: Segmental bone defect is a challenging clinical problem that often requires autologous bone grafting, which has limitations such as donor site morbidity and insufficient supply. Bone tissue engineering aims to create functional bone substitutes that can mimic the properties and processes of native bone. However, the discrepancy between *in vitro* and *in vivo* conditions hinders the successful translation of bone tissue engineering from animal models to human applications. Organoids, such as muscle pouch-based models, are emerging as promising tools that can closely resemble the osteogenic niche and overcome some of the limitations of conventional *in vitro* models.

Methods: In this study, we explored two distinct muscle-biomaterial based bone induction models: an *in vivo* heterotopic implantation model and a novel *ex vivo* muscle pouch-based coral-derived macroporous construct organoid model. They both utilized the coral-derived constructs, specifically 13 % hydroxyapatite/calcium carbonate (13 % HA/CC) as the biomaterial. We implanted 72 coral-derived devices into rats' *rectus abdominis* muscle, divided equally between *in vivo* and *ex vivo* groups. Samples were harvested at 15, 30, and 60 days for molecular and histological analyses. We assessed the relative gene expression of angiogenesis markers (*Vegfa* and *Col4a1*) and osteogenesis signaling and structural markers (*Runx2*, *Bmp2*, *Ocn* and *Alp*) using qRT-PCR. We analyzed tissue morphogenesis, angiogenesis and induction of bone formation by H&E and modified Goldner's Trichrome staining. Immunostaining was further used to detect the expression and localization of OCN, VEGFA and CD31 in both *in vivo* and *ex vivo* models.

Results: We demonstrated that *ex vivo* muscle pouch-based coral-derived macroporous construct organoid model supported tissue survival up to 60 days with compromised tissue ingrowth compared to the *in vivo* model. Primary vascular structures formed at the tissue–scaffold interface in the organoid system with persistent up-regulation of *Vegfa* and *Col4a1,* while comprehensive angiogenesis took place with early up-regulation of *Vegfa* and *Col4a1 in vivo*. Proper bone formation was absent in both the *ex vivo* and *in vivo* models, but the *in vivo* models showed an up-regulation of *Bmp2* and *Alp* in early phase and a delayed *Ocn* expression on day 30. The *ex vivo* model showed connective tissue formation, comprehensive OCN deposition, and gene expression patterns mimicking *in vivo* trends but with some distinctions.

Conclusions: The *ex vivo* muscle pouch-based coral-derived macroporous construct organoid model in this study can partially recapitulate angiogenesis and osteogenesis as compared to the *in vivo* model. However, key molecular signaling events that regulate these processes remained inactive. The study demonstrated that activating these events could enable the establishment of an *ex vivo* tissue-based vascularized model.

This article is part of a special issue entitled: Organs-on-chips and Organoids published in Journal of Orthopaedic Translation.

* Corresponding author. School of Clinical Medicine - Internal Medicine, Faculty of Health Sciences, University of the Witwatersrand, 7 York Road, Parktown, Johannesburg, 2193, South Africa.

** Corresponding author. Department of Orthopedics, Renji Hospital, School of Medicine, Shanghai Jiao Tong University, 160 Pu-Jian-Lu, Shanghai, 200127, China.

E-mail addresses: roland.klar@wits.ac.za (R.M. Klar), hetao@renji.com (T. He).

[1] These authors have contributed equally to this work and share first authorship.

https://doi.org/10.1016/j.jot.2025.04.002
Received 25 December 2024; Received in revised form 26 February 2025; Accepted 2 April 2025
Available online 26 April 2025

The translational potential of this article: This study partly elucidated the molecular signaling events involved in the development of an *ex vivo* tissue-based osteogenic organoid that closely resembled its *in vivo* counterpart. This would facilitate the development of well vascularized artificial bone grafts for treating segmental bone defects.

1. Introduction

Tissue engineering and regenerative medicine, which seek to restore both the function and structure of the original tissues/organs, has been under development for nearly nine decades [1–14]. Although, many tissue engineered techniques are reported, few have been successfully translated from functional animal or *ex vivo* based models into clinical applications, especially in the field of bone tissue engineering [15–17].

The classical approach for bone tissue engineering features osteoprogenitor cells and osteoinductive agents such as growth factors, mechanical stimulation, chemical stimuli, and geometrical signaling cues [18–22], combined with a suitable substratum, as stipulated in the bone induction principle [4,5,23], which together should mimic the properties of mature bone tissue and thereby recapitulate the induction of bone formation [24].

To date, various *in vitro* bioreactor models have been tested, among which organoids are increasingly exhibiting their exclusive advantages of not only better simulating the *in vivo* micro-environment, but also further recapitulating the repair and regeneration process [25,26]. Whilst different organoid models have been established in the last two decades, including intestinal, liver and lung organoids [27–29], few osteogenic organoid systems based on developmental engineering principles have been reported. However, muscle pouch-based models are emerging as a promising model for evaluating the osteogenic potential of biomaterials, as they can initiate and semi-imitate tissue wound repair cascades, mediating the orderly regulation of related genes including the release of various cytokines, thereby achieving true tissue regeneration [30–32]. Unlike classical bioreactor culture systems, which compose stem cells and scaffolds, muscle tissue provides not only mesenchymal stem cells, but also the raw material for synthetic metabolism. Muscle tissue contains essential amino acids, including specific signaling molecules, extracellular matrix and vascular structure, which more closely resemble the delicate osteogenic niche [33–35]. This enables *ex vivo* tissue like muscle tissue to closer resemble the true *in vivo* complicated micro-environment making such tissue-based *ex vivo* models superior to standard cell-based culture systems [33–36]. Furthermore, the muscle pouch-based osteogenic organoid system has been validated for long term survival showing robust angiogenesis potential *in vitro*, indicating its advantages over classic cell-based osteogenic bioreactor systems [37].

Numerous biomaterials have been demonstrated as promising candidates for bone-tissue-engineering applications, among which the most used are polymers, bioceramics and composite materials [21,38–41]. Coral-derived hydroxyapatite, primarily the genus Goniopora [42–44], is widely used in bone defect repair in laboratories, and remains one of the few known spontaneously bone inductive biomaterials [7,13,14,45,46] that is most similar to natural bone tissue with regard to both inorganic composition and spatial structure, continuous to serve as the ideal biomaterial for studying developmental bone tissue engineering research [47,48].

However, a chasm still exists between these *in vitro* based application and true bone formation regarding the exquisite process of natural regeneration or healing. To combat this problem, ever-increasing effort has been transferred from classical tissue engineering to developmental engineering, referring to a biomimetic tissue engineering strategy, to recapitulate the tissue or organ regeneration process while maintaining physiological characteristics, including regulation, autonomy and robustness [49–51]. Approaches of mimicking the corresponding key stages of tissue development and suitable culture platforms can quickly and efficiently guide stem cells to differentiate into the cell lineage required for specific tissue/organ regeneration, to obtain graft tissues close to the physiological state, and ultimately facilitate bench-to-bed translation [52–56].

In this study, we assessed how an *in vivo* heterotopic implantation model differs from its exact *ex vivo* muscle pouch-based coral-derived macroporous construct organoid counterpart, using a known spontaneously osteogenic auto-inductive coral-derived construct, 13 % hydroxyapatite/calcium carbonate (13 % HA/CC), to explore the differences in tissue metamorphosis and relevant gene expression between models. Our global aim, through more systematic complex and intricate studies, is ultimately to elucidate the exact molecular signaling events during *in vivo* and *in vitro* based osteogenesis inductive studies to develop a novel *ex vivo* human tissue/organ-based model that responds equivalently as its *in vivo* counterpart.

2. Materials and methods

2.1. Study design

This study used two muscle-biomaterial bone induction models: (1) an *in vivo* heterotopic implantation model that is generally used to analyze the bone inductive potential of biomaterials [4,57,58] and (2) a novel *ex vivo* muscle pouch-based coral-derived macroporous construct organoid model with goal of replacing the *in vivo* model in the future [37]. Briefly, 13 % HA/CC were utilized as they are known to be one of the few spontaneous osteoinductive materials and should exhibit differences between tissue ingrowth, angiogenesis and osteogenesis both molecularly and histologically between the two models.

72 coral-derived 13 % HA/CC devices were implanted into 12 rats' *rectus abdominis* muscle tissue pouch model and then separated randomly into an *in vivo* heterotopic implantation group (n = 36) and *in vitro* muscle pouch organoid culturing group (n = 36). Implantation specimens for each group were harvested equally after 15, 30 and 60 days (n = 12 per time point). Normal *rectus abdominis* muscle tissue, without implants, served as the endogenous control to which all samples were normalized. Half of the specimens from each time point (n = 6) underwent quantitative real-time reverse-transcription polymerase chain reaction (qRT-PCR) with the other half (n = 6) analyzed histologically (Fig. 1).

2.2. 13 % HA/CC (coral-derived) devices

The 13 % HA/CC (Zimmer Biomet, Warsaw, IN, USA) resulted from limited conversion of calcium carbonate ions that are replaced during the hydrothermal exchange by phosphate ions to generate calcium phosphate or as it is more commonly known hydroxyapatite [47]. The 13 % HA/CC device was a disc with a diameter of 5 mm and a thickness of 3.5 mm. The average solid trabeculae components' diameter of the 13 % HA/CC replicas was 130 μm, and their interconnections averaged 220 μm in diameter; the average porosity was 600 μm, and their interconnections' diameter was 260 μm on average [7].

2.3. Surgical device implantation setup

12 Fischer 344/DuCrl adult male rats, purchased from Shanghai SLAC Laboratary Animal Co. Ltd were used in this study. All practical experimental steps were performed in keeping with the rules and regulations of the Animal Protection Laboratory Animal Regulations (2013) and approved by the Animal Care Committee of Renji Hospital (Shanghai, China, No.: 201606230235). The Shanghai Renji Hospital

offered the animals' feeding sites and the place for animal experiments. No muscle tissue was purchased commercially or otherwise. 72 coral-derived 13 % HA/CC devices were used in total and equally split between animals. Subsequently, animals were likewise split equally between *in vivo* and *ex vivo* heterotopic implantation groups and experiments were done as follows.

2.3.1. In vivo heterotopic implantation model

Prior to surgical heterotypical implantation, 36 coral-derived 13 % HA/CC devices were prepared by immersing them in normal growth medium composed of Dulbecco's modified Eagle medium–high glucose (DMEMhg, Gibco, New York, USA), 40 IU/mL penicillin (Gibco) and 40 IU/mL streptomycin (Gibco). For each implantation time length, i.e., 15, 30 and 60 days, two animals were used with each animal receiving six implantations in total. On the day of surgery, six animals were injected intraperitoneally with 1 % pentobarbital (Fude Chemical Co., LTD, Shanghai, China) and sustained in the prone position under gas anesthesia ventilated with 1.5 % isoflurane (1.5 L/min, Abbot, Chicago, USA) for 15 min. The abdomen hair was shaved and a longitudinal incision was performed in order to expose the *rectus abdominis*. The 13 % HA/CC devices were then immediately implanted in intramuscular *rectus abdominis* pouches created by sharp and blunt dissection after which the fascia and skin incisions were then closed via the single-knot technique [37,46]. On day 15, 30 and 60 the relevant animals were euthanized using an overdose of isoflurane gas (Abbot, Chicago, USA), whereupon the relevant implanted specimens where then excised from the *rectus abdominis* muscle and the soft tissue was irrigated with sterile saline using 8 mm biopsy punches (PFM medical, China). Fresh muscle tissue without 13 % HA/CC devices was also harvested which acted as normalization controls.

2.3.2. Ex vivo muscle pouch-based coral-derived macroporous construct organoid model

For the *ex vivo* model, we used our previous standardized implantation system as established in He et al., 2020. 36 coral-derived 13 % HA/CC devices were prepared by immersing them in normal growth medium composed of DMEMhg (Gibco), 40 IU/mL penicillin (Gibco) and 40 IU/mL streptomycin (Gibco). Rats were then killed by an overdose of isoflurane, whereupon coral-derived 13 % HA/CC devices were implanted into intramuscular *rectus abdominis* pouches created by sharp and blunt dissection (He et al., 2020). The soft tissue was irrigated with sterile saline to prevent drying out of the tissue. Once all coral-derived 13 % HA/CC devices had been implanted, the relevant pouches with implants were excised with 8 mm biopsy punches (PFM medical) and placed into DMEMhg (Gibco) with 40 IU/mL penicillin (Gibco) and 40 IU/mL streptomycin (Gibco). The 36-muscle pouch-13 % HA/CC complexes were subsequently divided into 3 culturing periods set at 15 (n = 12), 30 (n = 12) and 60 (n = 12) days. Muscle tissue without 13 % HA/CC devices was also cultured in parallel to tissue pouches and acted as the normalization controls. Medium was changed every 2 days.

After the allotted culturing or growth period, *in vitro* and *in vivo* respectively, had been reached, i.e., 15, 30 or 60 days, all specimens were harvested. The 12 specimens, from each time point between the 2 models, were then randomly selected and either flash frozen in liquid nitrogen for qRT-PCR assays (n = 6 for each time point) or fixed in 4 % paraformaldehyde (Servicebio, Wuhan, China) to be processed for histological and histomorphometric analysis (n = 6 for each time point). The specimens for the histological assessment were further halved into 2 parts, with one half being processed for hard tissue section (non-decalcified) and the other half for decalcified section.

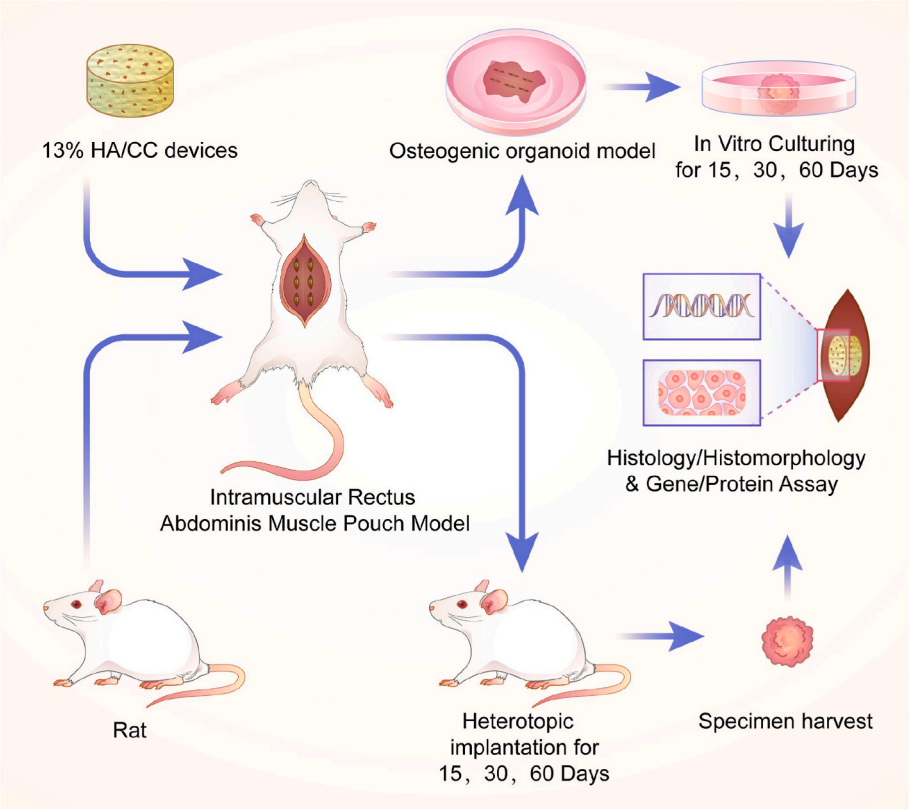

Fig. 1. Schematic diagram of the establishment of *in vivo* heterotopic implantation model and *ex vivo* muscle pouch-based coral-derived macroporous construct organoid model. 13 % HA/CC microporous devices were implanted into the *rectus abdominis* muscle pouch of rats and either maintained *in vivo* as the heterotopic implantation model or dissected and cultured *in vitro* as the *ex vivo* organoid model. Analysis was performed between the muscle-13 % HA/CC complex obtained from *in vivo* and *ex vivo* by histology/histomorphometry and gene expression/protein production assay. 13 % HA/CC, 13 % hydroxyapatite/calcium carbonate.

2.4. QRT-PCR

QRT-PCR was performed to determine the relative gene expression quantity of angiogenesis genes, vascular endothelial growth factor A (*Vegfa*) and collagen type IV alpha 1 chain (*Col4a1*), including known osteogenesis signaling and structural markers, runt-related transcription factor 2 (*Runx2*), bone morphogenetic protein 2 (*Bmp2*), osteocalcin (*Ocn*) and alkaline phosphatase (*Alp*), which together are critical determinants that are known to drive the induction of bone formation [37,59,60]. The primer sequences used in this study were selected from our previously established database [37,60] (Table 1). The specimens allocated for qRT-PCR assessment were ground to powder using liquid nitrogen. Total RNA was isolated using a modified RNA Trizol extraction procedure (Chomczynski and Mackey, 1995). Briefly, 1 mL Trizol (Invitrogen, San Diego, CA, USA) was added to the powdered tissue, where through the addition of chloroform (Sigma Aldrich, Wuxi, China) the aqueous RNA containing phase was transferred to Isopropanol (Sigma Aldrich). RNA was then pelleted out in an overnight centrifugation step at 4 °C, then washed with 75 % ethanol dried and resuspended in 32 μL RNase free water. A NanoDrop™ Lite (Thermo Scientific, Waltham, USA) was used to determine the RNA concentration and a Bioanalyzer 2100 (Agilent Technologies, CA, USA) was used to assess the quality. RNA integrity numbers (RIN) lower than eight were not accepted. RNA was then reverse transcribed into complementary DNA (cDNA) using the QuantiTect Reverse Transcription cDNA Synthesis Kit (Qiagen). QRT-PCR was performed with a LightCycler® 96 thermocycler (Roche) in duplicate with FastStart Essential DNA Green Master (Roche). The total reaction volume was 10 μL.

Each reaction contained 10 ng cDNA; 2x FastStart Essential DNA Green Master and 10 μM of each primer (Table 1). Primers were designed using Integrated DNA Technologies PrimerQuest Tool (https://eu.idtdna.com/Primerquest/Home/Index). Use of geNorm (https://www.researchgate.net/profile/Roland-Klar?ev=brs_overview) established that ribosomal protein lateral stalk subunit P0 (*Rplp0*), glyceraldehyde-3-Phosphate dehydrogenase (*Gapdh*), RNA polymerase II subunit e (*Polr2e*), actin beta (*Actb*), TATA-binding protein (*Tbp*), and ribosomal protein L13a (*Rpl13a*) were the most appropriate internal reference genes to use for *in vivo* group and *Rplp0*, *Gapdh*, *Polr2e*, *Actb*, *Tbp*, and succinate dehydrogenase complex flavoprotein subunit A (*Sdha*) for *in vitro* group.

The qRT-PCR thermocycling parameters included a preincubation of 3 min at 95 °C, followed by a three-step amplification program of 40 cycles consisting of a denaturation, annealing and extension step set at 95 °C for 10 s, 60 °C for 15 s and 72 °C for 30 s, respectively. Relative gene expression from the harvested muscle-device models was normalized against the six reference genes using Qbase + software (http://www.biogazelle.com) and fresh abdominal skeletal muscle tissue which was set as the endogenous control. Gene expression results are represented as mean calibrated normalized relative quantities (CNRQs) ± standard deviation (SD), which reflect the $\log_{10} 2^{-\Delta\Delta Ct}$.

Table 1
Primer sequences for target and reference genes.

Gene	Forward Primer (5′-3′)	Reverse Primer (5′-3′)
Vegfa	CTACCAGCGCAGCTATTG	GATCCGCATGATCTGCATAG
Col4a1	CTGGGAATCCCGGACTT	GGGATCTCCCTTCATTCCT
Runx2	CCCAAGTGGCCACTTAC	CTGAGGCGGTCAGAGA
Bmp2	GGAAGTGGCCCACTTAGA	TCACTAGCAGTGGTCTTACC
Alp	CGACAGCAAGCCCAAG	AGACGCCCATACCATCT
Ocn	GCGACTCTGAGTCTGACA	GGCAACACATGCCCTAAA
Rplp0 (reference)	CAACCCAGCTCTGGAGA	CAGCTGGCACCTTATTGG
Gapdh (reference)	CATGGGTGTGAACCATGA	TGTCATGGATGACCTTGG
Polr2e (reference)	GACCATCAAGGTGTACTGC	CAGCTCCTGCTGTAGAAAC
Actb (reference)	AGCTATGAGCTGCCTGA	GGCAGTAATCTCCTTCTGC
Tbp (reference)	TAACCCAGAAAGTCGAAGAC	CCGTAAGGCATCATTGGA
Rpl13a (reference)	TTTCTCCGAAAGCGGATG	AGGGATCCCATCCAACA
Sdha (reference)	GCGGTATGACACCAGTTATT	CCTGGCAAGGTAAACCAG

2.5. Histological and histomorphometric evaluation

As previously described [61], the specimens were fixed in 4 % paraformaldehyde (Servicebio) for 10 day at room temperature and dehydrated with increasing concentrations of ethanol. The specimens were then impregnated with a 1:1 mixture of absolute alcohol and Technovit 7200 VLC (Bio Optica Milano SpA, Milan, Italy) and embedded in pure Technovit 7200 VLC without decalcification. A microtome (Leica, RM2255, Germany) was used to cut 10 μm thick sections. Histological sections were stained then using either a hematoxylin-eosin (H&E) staining [62], or the modified Goldner (Jacques Goldner)'s Trichrome staining [63]. Stained sections were subsequently analyzed under Nikon Eclipse E100 microscopy (Nikon, Tokyo, Japan). The number and diameter of blood vessels of each sample from *in vivo* and *ex vivo* models were counted and calculated for each time-point. Goldner's Trichrome staining was performed for static histomorphometric measurement. The percentage of Goldner's Trichrome positive osteoid regions compared to the construct without peripheral muscle were analyzed with ImageJ v1.43 (ImageJ Software, Maryland, USA).

2.6. Immuno-histomorphometric assays

Specimens were fixed in 4 % paraformaldehyde (Servicebio) for 24 h, dehydrated using an increasing concentration of ethanol solutions, and finally embedded into paraffin wax. Prior to cutting 2 μm sections the surface of each paraffin block was decalcified [64]. For angio-/vasculogenesis and chondro-/osteogenesis evaluation, 2 μm-thick paraffin wax sections were incubated with primary antibodies to detect the presence of VEGFA and OCN. The primary antibodies of VEGFA and OCN (Biorbyt, Cambridge, UK) were diluted with antibody diluent (Abcam, Shanghai, China) at the concentration of 1:200 and 1:100, respectively, determined by serial dilution pre-test with rat abdominal skeletal muscle set as positive control. The antigen–antibody interactions of each protein assay were shown by Vina Green™ Chromogen Kit (Biocare Medical, CA, USA). Stained specimens were analyzed under Nikon Eclipse E100 microscope (Nikon). Three tissue samples per group were used for immune-histomorphometry. Positive protein production was characterized as green staining of the regions. For histomorphometric assessment of VEGFA and OCN, the absorbance value of the incident light in the blank area of specimens was calibrated. The mean optical density (MOD) was determined by measuring of integrated optical density (IOD) divided by the region of interest (ROI) (MOD = IOD/ROI). MOD represented the corresponding value of the relative strength of antigenicity in the relevant sections.

2.7. Immunofluorescence analysis

The dehydrated and decalcified specimens were cut into 5 μm thick sections for immunofluorescence staining. After treatment with citrate antigen retrieval solution (Servicebio) and washing by phosphate-buffered saline, the sections were incubated with immunostaining blocking solution for 30 min at room temperature. Then the sections were incubated with anti-CD31 primary antibody (1:300, Servicebio) and anti-VEGFA antibody (1:300, Servicebio) overnight at 4 °C, followed by incubating with the corresponding fluorescein-conjugated secondary antibodies (Servicebio) for 50 min at 37 °C. 4′,6-diamidino-2-phenylindole (DAPI, Servicebio) was used to stain cell nuclei for 10 min at room temperature. The slides were mounted in an anti-fade mounting medium. Stained specimens were captured under Nikon Eclipse E100 microscope (Nikon) and analyzed using ImageJ v1.43 (ImageJ Software, Maryland, USA) to compare mean gray value (mean gray value = integrated density/ROI).

2.8. Statistical analysis

Data were analyzed using GraphPad Prism v8.0.1 (GraphPad Software, San Diego, USA). The results were represented as mean ± SD. Measurements were performed in histomorphometric (n = 6), immunohistomorphometric/fluorescent analyses (n = 3) and qRT-PCR (n = 6), respectively. The one-way ANOVA and Scheffé's multiple comparison are used to determine statistical significance. Statistical significance was indicated by * for $P < 0.05$, ** for $P < 0.01$ and *** for $P < 0.001$.

3. Results

3.1. Ex vivo muscle pouch-based coral-derived microporous construct organoid model supported long-term tissue survival with compromised tissue ingrowth compared to in vivo model

The H&E staining results of heterotopic implantation of 13 % HA/CC into the muscle pouch (Fig. 2 A–H) indicated that the areolar connective tissue penetrated and was comprehensively distributed within the macroporous devices on day 15 compared to day 0 (Fig. 2 A and C). From the higher magnification (Fig. 2 D), a characteristic distribution of dense cellular deposition at the interface of devices (Fig. 2 D, green arrow) in contrast to sparse cells located within connective tissue matrix was observed while primary vessels were present deep within the center of the device (Fig. 2 D, blue arrow). On day 30, the cell density had significantly increased compared to that of day 15, with widely disseminated mature vessels within the tissue (Fig. 2 E and F, blue arrows). Multinucleated giant cells (Fig. 2 E, green arrow) were detected near the blood vessels in the concave space of the macroporous constructs. *In vivo* results by day 60 (Fig. 2 G and H) illustrated the deposition of condensed collagen fibers (Fig. 2 H, blue arrows) that mainly lined at the interface of the coral-derived constructs supported with the evenly distributed blood vessels (Green arrows). In contrast to the *in vivo* model, the *ex vivo* organoid model depicted that although connective tissue grew into the center of the construct (Fig. 2 K and L), it failed to properly develop and survive properly over time, illustrating mainly

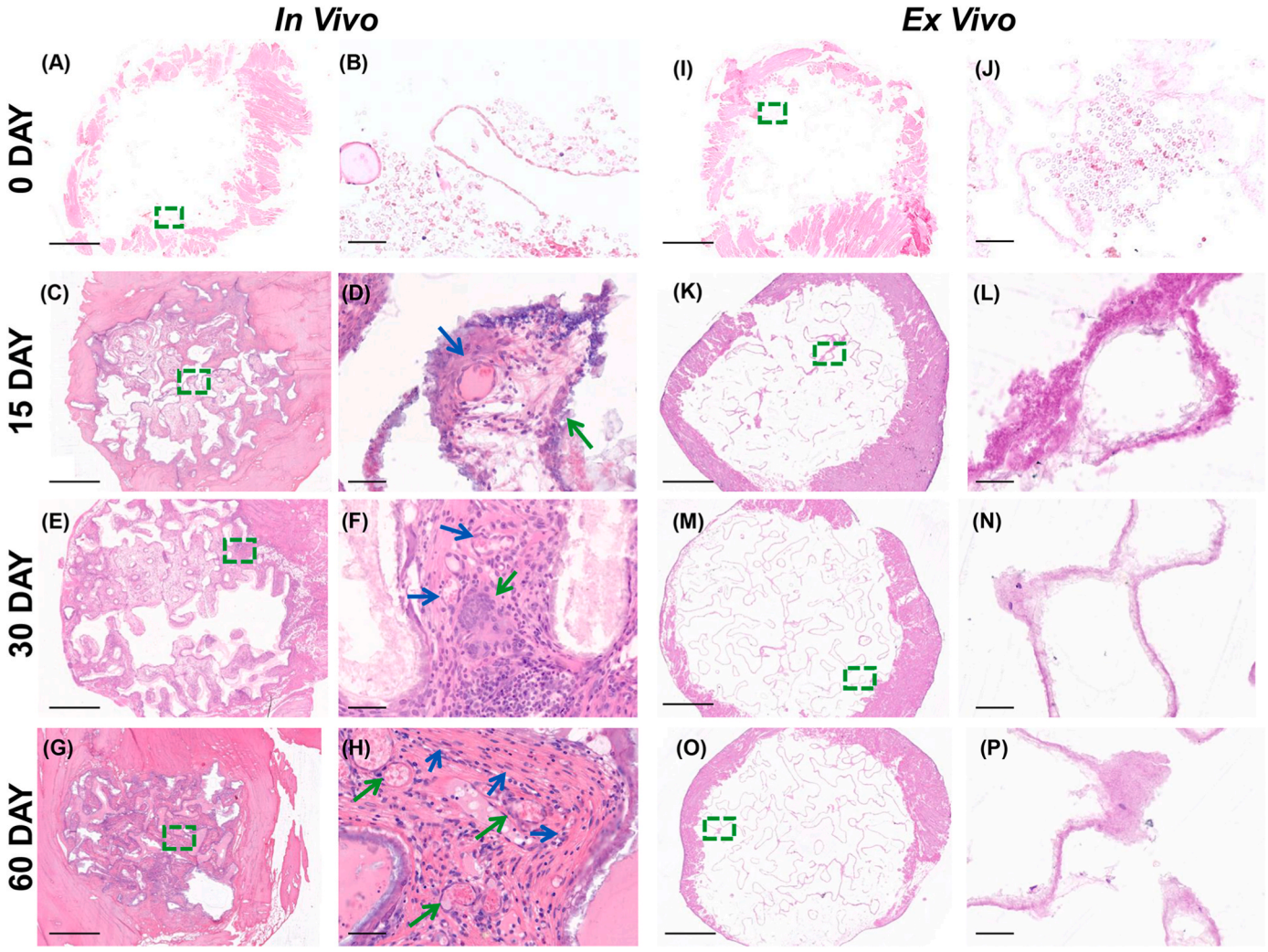

Fig. 2. Comparison of tissue survivability and growth between the *in vivo* and *ex vivo* muscle pouch-based coral-derived macroporous construct organoid models on day 0, 15, 30 and 60 (A–P). *In vivo* models (A–H) revealed that the invasion of connective tissue was broadly distributed within the macroporous devices on day 15 compared to day 0 (A, C). At higher magnification (D), a distinctive distribution of dense cellular deposition was observed at the interface (D, green arrow), in contrast to sparse cells found within the connective tissue matrix, whereas principal vasculature was found in the central zone (D, blue arrow). The cell density was much higher on day 30 compared to day 15, and mature vessels were broadly distributed throughout the tissue (E and F, blue arrows). Multinucleated giant cells (F, green arrow) formed near blood vessels in the concave space of the macroporous constructs. *In vivo* results by day 60 (G, H) depicted abundant vessels uniformly distributed within the firm connective tissue in the central region (H, green arrows) supporting the substantial formation of condensed fibers lining mainly at the interface of the constructs. In *ex vivo* organoid model, compared to Day 0 (I, J), connective tissue grew into the center of the construct on Day 15 (K, L), but failed to survive and develop over time with scattered live cells mainly deposited in the peripheral area (M, N). Nevertheless, tissue survival of *in vitro* culturing with viable cells deposited within the extracellular matrix can last up to 60 days (O, P). H&E staining. Scale bars: A, C, E, G, I, K, M and O = 1 mm; B, D, F, H, J, L, N, and P = 50 μm.

some scattered live cells deposited in the peripheral area (Fig. 2 M and N). Despite the limited tissue growth deep into the construct, the *ex vivo* organoid model achieved survival *in vitro* culturing with viable cells deposited within the extracellular matrix up to 60 days (Fig. 2 O and P).

3.2. Comprehensive vascularization took place in vivo while primary vascular structures occurred in ex vivo organoid models

The results of Fig. 3 A–C depicted that capillaries formed within the pores of the coral derived scaffold supported by areolar tissue on day 15 *in vivo* (Fig. 3 A, green arrow**)** with upregulated expression of *Vegfa* and *Col4a1* (Fig. 3 I). By day 30, the number of blood vessels significantly increased ($P < 0.01$) (Fig. 3 B**,** green arrows; G). Intriguingly, *Vegfa* and *Col4a1* were downregulated significantly (Fig. 3 J) at this timepoint ($P < 0.05$); On day 60, the number of blood vessels tended to increase further (Fig. 3 G) with significant larger diameter ($P < 0.05$) (Fig. 3 H) and blood vessel bundles were formed (Fig. 3 C**,** blue arrow) with the persistently downregulated expression of *Vegfa* and *Col4a1* (Fig. 3 K). In comparison, in the *ex vivo* muscle pouch-based coral-derived macroporous construct organoid model, vascular structures were observed at the tissue-scaffold interface on day 15 (Fig. 3 D**,** green arrow) and survived by day 30 (Fig. 3 E**,** green arrow) as relatively small vessels (Fig. 3 H), but without the presence of blood vessels within the scaffold. On day 60, we observed a blood vessels-like structure (Fig. 3 F**,** green arrow), and further VEGFA protein synthesis via immunohistochemical assay (Fig. 4 A–D, Supplementary Figure 1) confirmed the presence of primary blood vessels within the scaffold which was supported by the continuous up-regulation of *Vegfa* and *Col4a1* (Fig. 4 E and F). Persistent *Col4a1* expression (Fig. 4 E) suggests delayed basement membrane formation *ex vivo*, correlating with immature vasculature (Fig. 3 F). Compared with

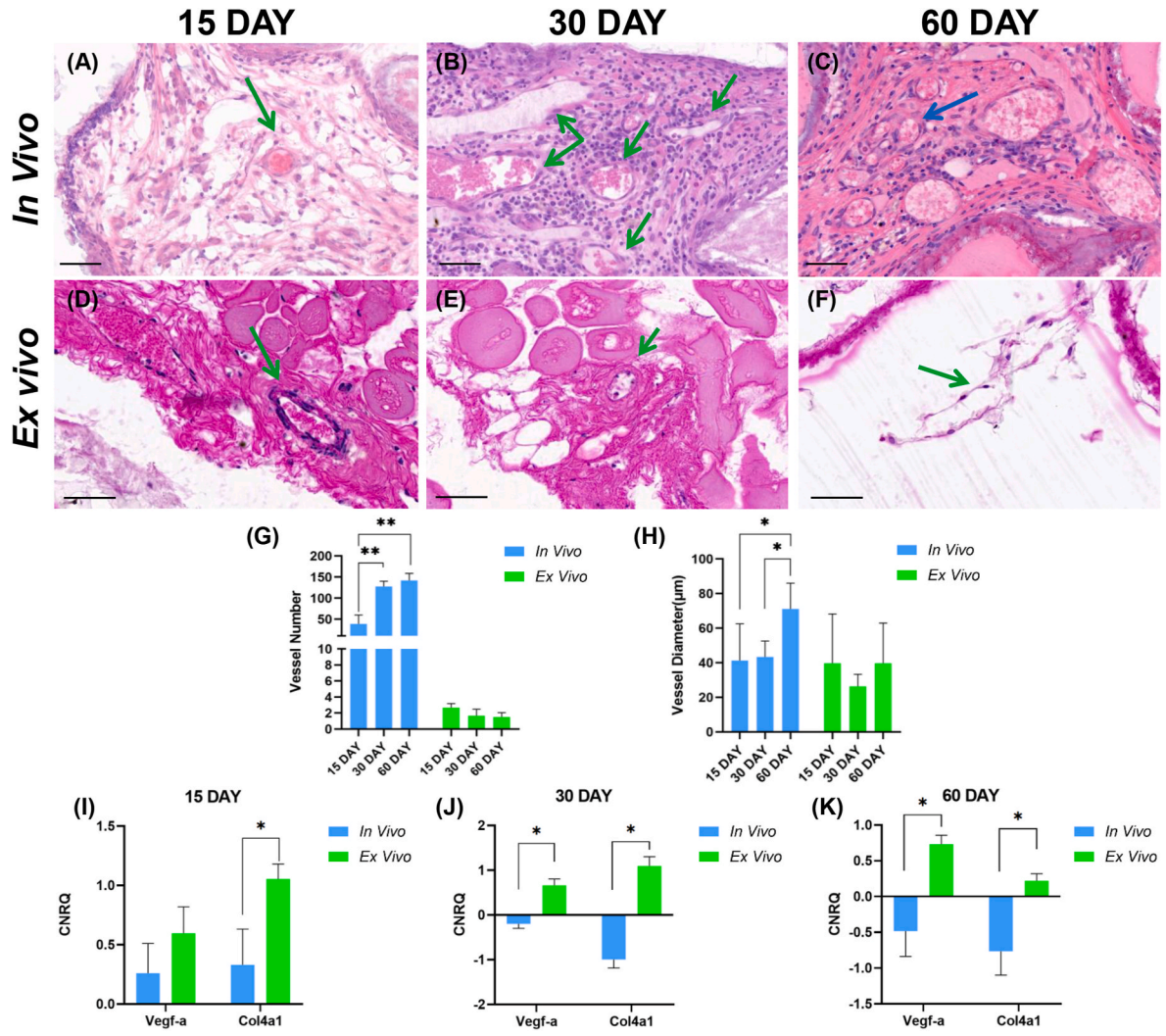

Fig. 3. Comparison of vasculogenesis between the *in vivo* and *ex vivo* muscle pouch-based coral-derived macroporous construct organoid models on day 15, 30 and 60 (A–K). On day 15 in the *in vivo* model, morphology showed capillaries formed within the pores of the coral-derived scaffold supported by areolar tissue (A, green arrow), indicating upregulated expression of *Vegfa* and *Col4a1* (I). By day 30, the number of blood vessels increased (B, green arrow). Meanwhile, *Vegfa* and *Col4a1* expression was dramatically downregulated (J); on day 60, the number of blood vessels increased even more and blood vessel bundles were formed (C, blue arrow), despite the continued downregulation of *Vegfa* and *Col4a1* (K). A significant increase of the number and diameter of blood vessels was noted on day 60 compared to the early phase within *in vivo* models by quantitative histological analysis (G, H). Vascular structures were visible at the interface on day 15 (D) and survived by day 30 (E) in the *ex vivo* muscle pouch-based coral-derived macroporous construct organoid model, although there were no blood vessels within the 13 % HA/CC scaffold. Some blood vessel-like structures were observed on day 60 (F). Quantitative histological analysis of vessel numbers (G) and vessel diameters (H) showed very limited numbers of relatively small vessels within *ex vivo* organoid models without significance over time. *Ex vivo* organoid model demonstrated continuous upregulation of *Vegfa* and *Col4a1* on day 15, 30, and 60, and *in vivo* results revealed early upregulation and later inhibition (I, J, K). H&E staining (A–F). Error bars are Mean ± SD. *, $P < 0.05$. Scale bars: A, B, and C = 50 μm; D, E and F = 50 μm. 13 % HA/CC, 13 % hydroxyapatite/calcium carbonate; CNRQs, calibrated normalized relative quantities.

the *ex vivo* organoid model, in which *Vegfa* and *Col4a1* were continuously upregulated on day 15, 30, and 60, the *in vivo* results showed the characteristics of early upregulation and later inhibition which falls in line with how bone formation by induction normally occurs *in vivo* (Fig. 3 I and J and K). Immunofluorescence assays of VEGFA and CD31 within 13 % HA/CC showed limited VEGFA and CD31 production via different cells without apparent vasculature formation *in vitro* (Fig. 5 A–C). In comparison, early vessel formation and mature vascular network formation over time were noted *in vivo* (Fig. 5 D–F). Quantitative analysis revealed the continuous production of VEGFA and CD31 at lower levels *in vitro*, while that of *in vivo* at a higher level with significant increase of CD31 production over time (Fig. 5 G–J).

3.3. *In vivo heterotopic implantation model supported tissue morphogenesis within the coral-derived constructs while ex vivo organoid model revealed similar potential*

Histological analysis revealed specific tissue morphogenesis in the macroporous spaces of the coral-derived device within the *in vivo* heterotopic implantation model by day 60 (Fig. 6 A–D). 13 % HA/CC induced pattern formation and a highly vascularized mesenchymal tissue (Fig. 6 A and B, blue arrows) with firm connective tissue and condensed collagen fibers (green arrows) deposited at the interface of the constructs. In some concave spaces of the macroporous constructs, condensed fibers transitioned to a homogeneous tissue layer, with cells entrapped within the tissue (Fig. 6C and D, red arrow). Gene expression assay revealed that *Bmp2* expression peaked on day 15 and significantly decreased over time (Fig. 6 E). A similar regulatory pattern was observed for *Alp* (Fig. 6 F) as well, aligning with physiological osteoinduction patterns. However, *Ocn* expression was upregulated on day 15 and peaked on day 30, whereafter a significant downregulation by day 60 was observed (Fig. 6 G). By quantitative histological analysis of Goldner's trichrome stainings (Fig. 6H), significant increase of osteoid area was noted on day 30 ($P < 0.05$) and day 60 ($P < 0.01$) compared to day 15 within *in vivo* models, while lower percentage of osteoid area was observed over time in *ex vivo* organoid models.

The results obtained from the *ex vivo* muscle pouch-based coral-derived macroporous construct organoid model, as shown in Fig. 7 revealed that connective tissue formed near the interface of the macroporous spaces (Fig. 7 A and B) after 60 days of *in vitro* culturing. Immuno-histological assay depicted a comprehensive OCN deposition within the construct on day 60 (Fig. 7 C and D) and a significant histomorphometric increase over time (Fig. 7 F). *Bmp2* was upregulated throughout the culturing period and exhibited a downward trend similar to that observed *in vivo*. Contrarily, *Alp* was downregulated over time, suggesting delayed osteoblast differentiation due to incomplete signal transduction. *Ocn* was significantly upregulated from day 30 and maintained to day 60 suggesting the presence of mature osteoblasts

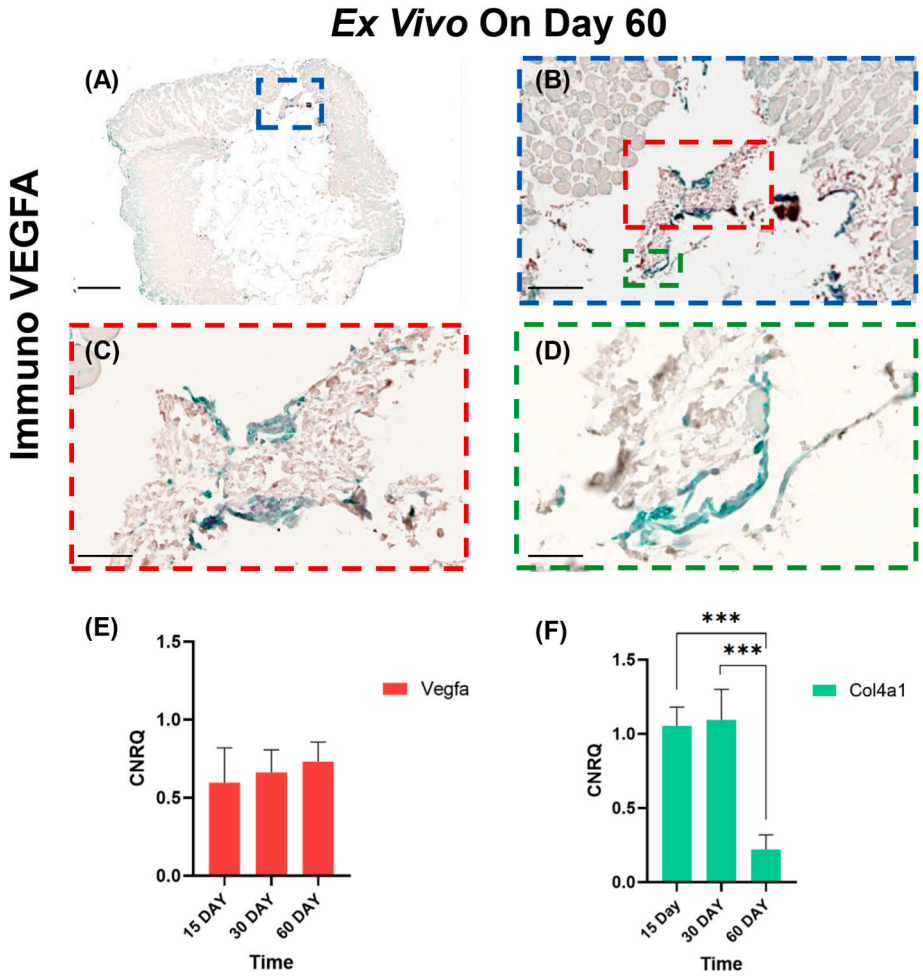

Fig. 4. Immunohistological and gene expression analysis of vasculogenesis in *ex vivo* muscle pouch-based coral-derived macroporous construct organoid model. Immunohistological analysis of VEGFA protein production within the coral-derived constructs illustrated the presence of blood vessels in the *ex vivo* organoid model on day 60 (A–D). Meanwhile, the expression of angiogenic gene markers (*Vegfa* and *Col4a1*) was continuously upregulated over time (E, F). Decalcified sections cut at 2 μm underwent immunohistological analysis of VEGFA. Error bars are Mean ± SD. ***, $P < 0.001$. Scale bars: A = 1 mm; B = 200 μm; C = 100 μm; D = 50 μm. CNRQs, calibrated normalized relative quantities.

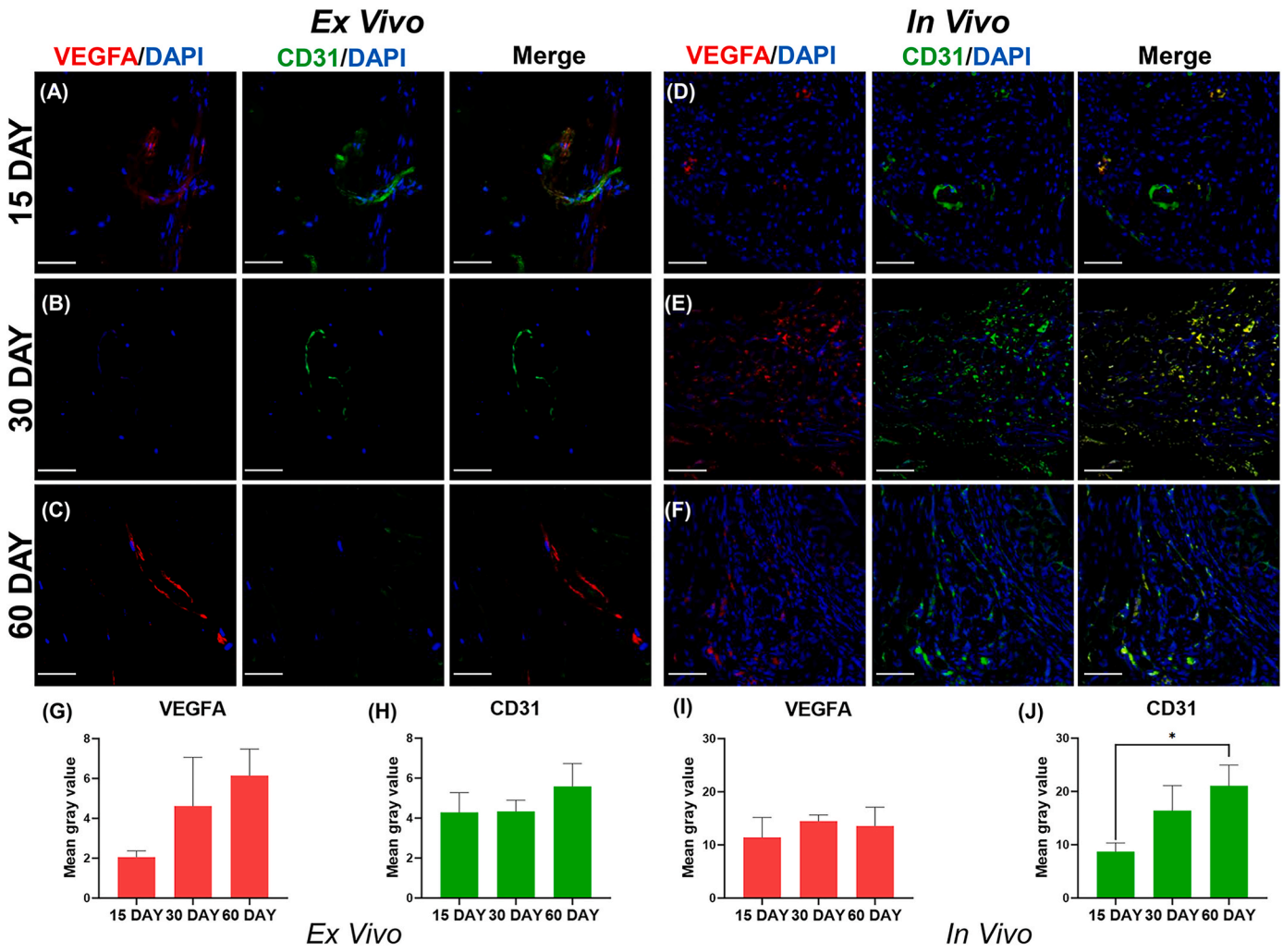

Fig. 5. Immunofluorescence analysis of vasculogenesis within 13 % HA/CC over time in the *ex vivo* and *in vivo* models. Immunofluorescence staining of VEGFA and CD31 protein production within the coral-derived constructs identified limited VEGFA and CD31 production by different cells without vasculature formation *ex vivo* (A–C) compared to the early vessel formation (D) and mature vascular network formation over time (E, F) *in vivo*. Quantitative analysis (G–J) depicted the continuous production of VEGFA and CD31 at lower level *ex vivo* (G, H), while that of *in vivo* at a higher level with significant increase of CD31 production over time (I, J). Error bars are Mean ± SD. *, $P < 0.05$. Scale bars: A-F = 50 μm. 13 % HA/CC, 13 % hydroxyapatite/calcium carbonate; VEGFA, vascular endothelial growth factor A.

contributing to the matrix mineralization process, while *Runx2* was always upregulated (Fig. 7 E).

4. Discussion

The principles of bone tissue engineering have changed little over the years since their initial description nearly six decades ago by Marshal Urist's leading science article "Bone: formation by autoinduction" [4] with the idea of regenerating bone in humans as old as two millennia [65,66]. Using a series of heterotopic intramuscular implantations, by means of an allogeneic demineralized bone matrix, in conjunction with a rodent calvarial orthotopic defect site, Urist (1965) [4] described the process of autoinduction in great detail. This provided the foundation for what has become the fundamental process by which scientists are still eluded to properly reproduce clinically. Vast amounts of time and research have been expended towards unravelling one of the nature's greatest biological secrets that is the proper induction of bone reformation as recapitulated by the gold standard, the bone autograft [67–70].

The animal-based bone regeneration experimental model is ever more becoming unreliable to work with, simply because the results cannot be translated towards a clinical setting [71,72]. However, as opposed to testing new therapies or materials based on the tissue induction principle [4,5,10,65], the intended mode of regeneration, as observed in animals, is utilized to establish the chronological order of the exact spatial and temporal signals involved in tissue formation. Not only would this provide us with a means to initiate "clinical trials" without endangering any humans, but, more importantly, by using this system to grow bone through the formation by autoinduction *in vitro*. This would perhaps finally allow us to properly recapitulate true bone formation restricted currently to the autogenous bone graft [4,25,57,73].

In the study presented here we attempted the first steps to "Bone: formation by autoinduction *ex vivo*". Under the circumstances this was a highly challenging task, as there remains little knowledge on the full extent of what is fully required, the literature remains convoluted with diverse theories and suggestions [74–76], for the process to be recapitulated. We thus tried to remain true to the foundations of the bone induction principle [4,5,10,23], conducting an informative yet simple study that would provide critical information, from which then, in future experiments, we can determine what else needs to be incorporated to get the process to work properly.

The bone induction principle suggests incorporating an insoluble substratum with a soluble signal that then stimulates migration and

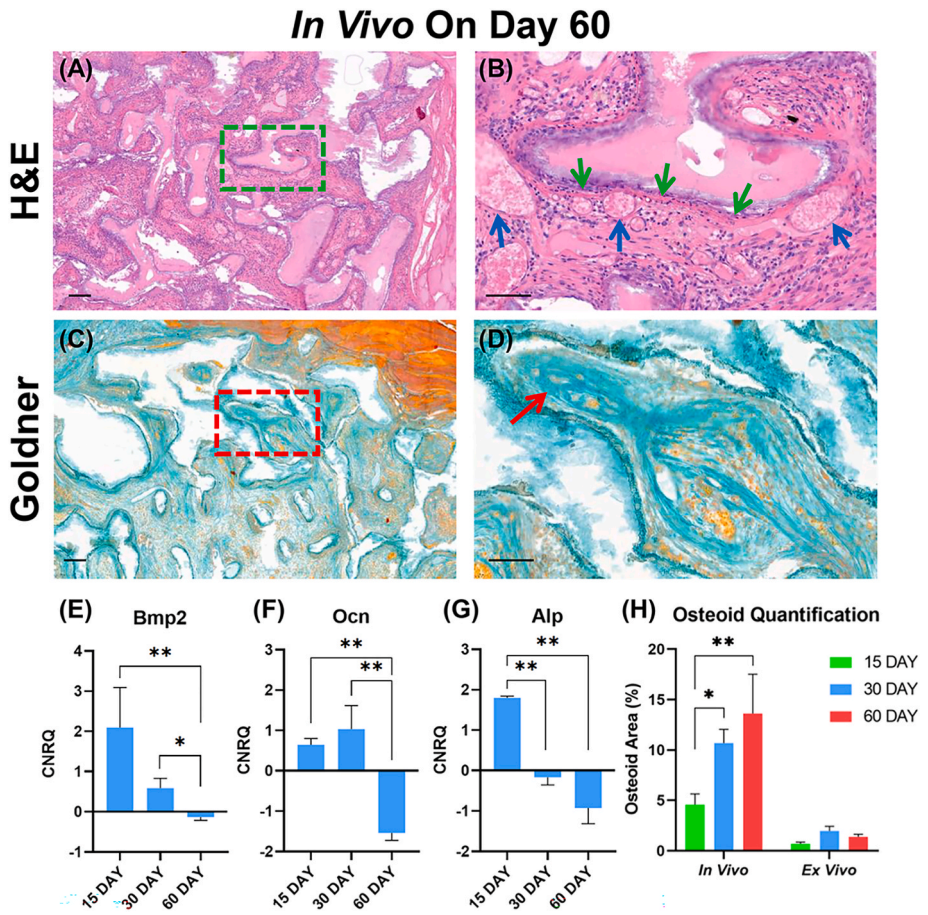

Fig. 6. Tissue morphogenesis within the *in vivo* heterotopic implantation model. Specific tissue morphogenesis patterns formed in the macroporous coral-derived devices within the heterotopic implantation model by day 60 (A–D). Mesenchymal tissue underwent condensation at the interface of the constructs (A and B, green arrows) with the support of abundant mature vessels (blue arrows). Transformation from condensed connective tissue to homogeneous tissue was observed in some concave spaces of the macro-porous constructs (C and D, red arrow). *Bmp2* peaked on day 15 and exhibited a considerable decline over time (E); *Alp* gene expression assay revealed a similar regulation pattern (G). *Ocn* expression was upregulated on day 15 and peaked on day 30, following significant down-regulation (F). By quantitative histological analysis of Goldner's trichrome stainings, significant increase of osteoid area was noted on day 30 and day 60 compared to day 15 within *in vivo* models while lower percentage of osteoid area was observed over time in *ex vivo* organoid models (H). H&E staining (A, B). Goldner's trichrome staining (C, D). Error bars are Mean ± SD. *, $P < 0.05$; **, $P < 0.01$. Scale bars: A, C = 200 μm; B, D = 100 μm. CNRQs, calibrated normalized relative quantities.

possibly even transformation of cells at the implantation site to undergo the process of bone formation [5,10,23]. The principle may need some adjustment, as it is widely accepted today that a soluble signal may not always be critical to initiate the bone formation cascade [75,77] because certain changes in calcium ion content [46,78] are all that necessary to achieve spontaneous bone formation. Numerous biomaterials have been utilized in bone tissue engineering and regeneration, which include, but are not limited to, collagen sponges [31], demineralized bone matrices [79], and hydroxyapatite scaffolds [80]. The spatial configuration of the scaffold is a vital property that determines whether the tissue can effectively grow into the scaffold [38]. Current studies have shown that macro-porous materials have better bone induction and conduction capabilities than micro-porous materials and thus support the extensive ingrowth of tissue and vasculogenesis [38,81,82]. The diameter of the pathway between macropores is, in particular, a key parameter. Only when the diameter is within the appropriate range (100–200 μm), can it ensure extensive formation of vascularized tissue and good bone formation [37,38]. Among the numerous biomaterials, evidence validated that coral-derived macroporous devices are composed of hydroxyapatite and have superior pore size and spatial configurations than any other known artificial biomaterial [7,38,45,83]. Previous studies have further confirmed that it has excellent bone formation inductivity, biocompatibility and osteoconductivity, which can be used not only to repair bone defects [14,84,85], but also can be implanted into the muscle ectopically to induce ectopic bone formation [7,13,14,46].

The "intramuscular" or "muscle pouch" implantation model is the standard *in vivo* model used to study and validate whether biomaterials can induce bone formation and through which processes [71,74,86]. Considering the viability of muscle tissue culture compared with that of bone tissue and the good osteogenic induction potential of muscle tissue, this became our model of choice *ex vivo* as it had previously exhibited great potential in determining biomaterial osteoinductivity [37]. By using this new *ex vivo* muscle pouch-based coral-derived macroporous construct organoid model, which simulates the classical *in vivo* heterotopic implantation model, the prospect of achieving "Bone: formation by autoinduction *ex vivo*" was investigated. We chose to keep track of events as they occurred to develop new insights into what our *in vitro* model would need in future experiments until true bone reformation is achieved.

In this study, we discovered firstly that the muscle pouch-13 % HA/CC-based organoid model could survive up to 60 days *in vitro*, which is significantly longer than any cell-based osteogenic organoid system, to date. Most organoid systems can maximally endure *in vitro* culturing up to four weeks [73,87,88]. As bone formation process *in vivo* needs at least 2–3 months to properly manifest itself, the extended survival time with the *ex vivo* organoid model provides sufficient time to allow for the

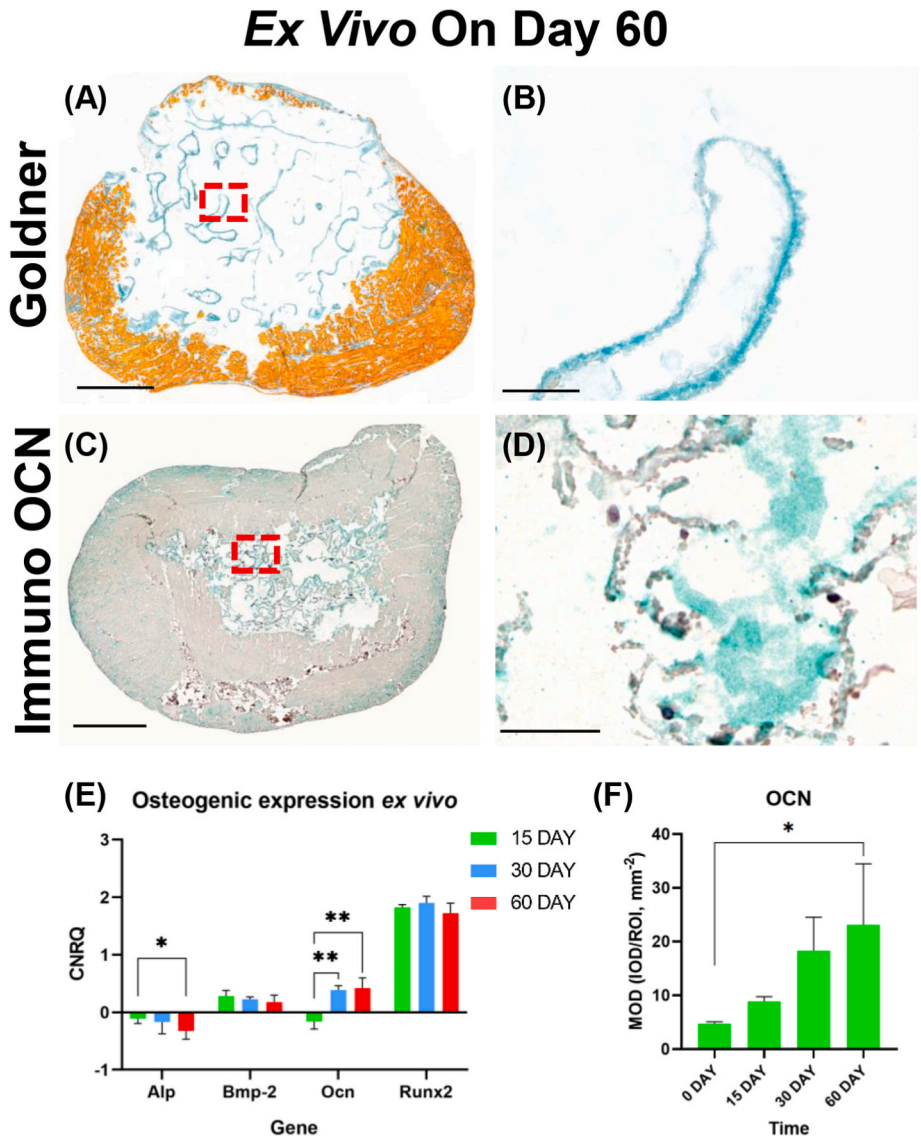

Fig. 7. Induction of osteogenesis within *ex vivo* muscle pouch-based coral-derived macroporous construct organoid model. On day 60 *ex vivo*, limited osteoid was formed at the interface of the macroporous spaces (A, B). Immunohistological assays depicted a complete OCN deposition within the 13 % HA/CC construct (C, D) and considerable histomorphometric increase over time (F). For gene expression analysis (E), *Bmp2* was upregulated with a decreasing tendency; *Alp* was consistently suppressed; *Ocn* was significantly upregulated from day 30 and last to 60 days; and *Runx2* was consistently upregulated at a high level. Goldner's trichrome staining (A, B). Decalcified sections cut at 2 μm underwent immunohistological analysis of OCN (C, D). Error bars are Mean ± SD. *, $P < 0.05$; **, $P < 0.01$. Scale bars: A = 1 mm; B = 100 μm. 13 % HA/CC, 13 % hydroxyapatite/calcium carbonate; CNRQs, calibrated normalized relative quantities.

possible recapitulation of bone formation. A tissue-based *ex vivo* culturing system shows its advantage over cell-based models, probably due to the better biomimicry of the *in vivo* environment, with the presence of micro-vessels, micro-nerves and other components intrinsically available within tissue that together cause a superior biological response [26]. Indeed, vascular-like structure formation was observed in the present *ex vivo* muscle pouch-based coral-derived macroporous construct organoid model, suggesting that tissue with remnant blood vessels can induce new angiogenesis/vasculogenesis. However, compared with the comprehensive tissue in-growth in the *in vivo* heterotopic implantation model, tissue growth restrained itself near the tissue–scaffold interface in the *ex vivo* organoid model.

One of the main reasons for the difference in tissue growth between the *in vivo* and *ex vivo* models may lie in the significant difference of vasculogenesis within the two models. Trueta and Buhr, (1963) [89] discerned that vasculogenesis was the primary guiding superstructure that creates a translucent form of the type of tissue that will be formed around the blood vessels. Without a proper vascular supply bringing in crucial nutrients and additional progenitor stem cells including the vital immunoreactive monocytes/macrophages, essential for driving bone formation [46,90], real bone reformation and remodeling would occur in a very limited quantity. Whilst we acknowledge that the formation of proper vasculogenesis and vessel penetration was a critical limitation, as well as the absence of monocytes in the *ex vivo organoid* model, it did show the presence of vascular-like structures on day 60 near the peripheries of the coral-derived scaffolds. Curiously, the expression of both *Vegfa* and *Col4a1* were continuously and gradually upregulated during the whole culturing period, suggesting that the call of vascularization by surrounding muscle tissue persisted in the *ex vivo organoid* model. This persistent upregulation contrasts with the *in vivo* model, where *Vegfa* and *Col4a1* expression exhibited a transient peak followed by down-regulation, reflecting the natural progression of vascular remodeling

and stabilization. The *in vivo Vegfa/Col4a1* expression pattern aligns with previous studies demonstrating that VEGFA plays a predominant role in early endothelial recruitment and permeability, whereas Col4a1 contributes to basement membrane formation and vascular maturation [91]. However, the production of angiogenic factors such as VEGFA and CD31 were lower within the organoid than *in vivo*, with few cells producing both factors, indicating limited migration or formation of vascular endothelial cells into the porous construct. Hence, it is plausible to suggest that the *in vitro* culturing system does not allow for the proper diffusion of both essential nutrients and critical signals across the tissue-biomaterial border. We theorize that medium changes continuously dilute resident signal concentrations which in turn prevent proper signal embedment within the inner matrix, except near the periphery. This would explain why tissue formation was primarily limited at the border of the coral-device *in vitro*.

Moreover, the static culture environment deviates from the physiological homeostasis with flow, failing to provide essential fluidic shear stress mechanical cues necessary for vessel maturation and vascular network formation [92]. Whilst it could also simply be a reduced rate of angiogenesis based on limiting nutrients and essential amino acids often lacking from *in vitro* culturing models [90], solving the enigma of proper and adequate vascularization within our *ex vivo* organoid model will need to be addressed in future experiments, as this is the foundation on which the subsequent bone formation occurs. This was properly exemplified in the *in vivo* model where vascularization started in the very early stage with blood vessels appearing within the macropores of the scaffold as early as day 15 and a comprehensive mature vascular network formed by day 60. The downregulation of angiogenic factors such as *Vegfa* and *Col4a1* in the later phase, after implantation, may lie in three aspects. First, angiogenesis is a highly organized series of events and requires precise spatial and temporal regulation of various angiogenic factors, including *Vegfa*, basic fibroblast growth factor-2 (*FGF-2*) and platelet-derived growth factor (*PDGF*). Among these factors, *Vegfa*, as a key early-phase regulator in angiogenesis, mainly aids in vascular permeability and endothelial cell recruitment, while *Col4a1* is critical in the basement membrane formation of new capillaries and partially also in endothelial tissue development [10,77,88,93]. Notably, although *Vegfa* is not an endothelial-specific marker, its dynamic expression synergizes with *Col4a1* to provide dual validation of angiogenic activity and structural maturation (Fig. 3A–C). For instance, *Vegfa*' s early peak (Day 15) drives endothelial proliferation, while persistent *Col4a1* expression (Day 30) marks basement membrane deposition, collectively supporting the "angiogenesis-maturation" transition [93–95]. As a widely used endothelial-specific marker, CD31 immunofluorescence (Fig. 5) further confirms endothelial presence, and its consistency with *Vegfa/Col4a1* trends confirmed early-phase vasculogenesis *in vivo* models [96]. Second, qRT-PCR is a relative quantification of gene expression level and in this study, fresh abdominal skeletal muscle tissue was set as the control. Therefore, the downregulation of *Vegfa* after 30 days of implantation only suggested that the transcriptional expression level of *Vegfa* and *Col4a1* were lower than those in untreated muscle tissue, rather than indicating the termination of angiogenesis within the system. Third, as we know, transcriptional regulation predates protein production and the subsequent morphological changes [97]. This is the natural known pathway taken for the formation of bone formation in which the reduction in *Vegfa* and *Col4a1* signaling over time indicates that proper vascularization and endothelial tissue matrices have been properly established. In addition, consistent increase of CD31 production indicates the maturation of the vascular network *in vivo*. This allows for more complex tissue formation processes either over the intramembranous or endochondral bone formation pathway [98].

Indeed, the lack of proper vascularization mirrored the results observed both *ex vivo* and *in vivo*. Prominent tissue morphogenesis, in the form of collagen condensations was observed within the macroporous constructs. This was primarily limited to the *in vivo* model. The *ex vivo* organoid model on the other hand exhibited little to no tissue invasion with OCN deposition only near the peripheral region. Curiously, the regulation pattern of *Ocn*, a late bone formation marker [99], was similar *ex vivo* and *in vivo*. This further substantiated our theory that the *ex vivo* organoid model functions at a slower rate with an insufficient response to the auto-inductive biomimetic constructs than the *in vivo* model, resulting in less tissue transformation and development, ultimately retarding or preventing bone formation.

Although the initial construction of both the *in vivo* and *ex vivo* models was the same, using the heterotopic implantation model [71,72,74], the outcomes were significantly different. We can with certainty state that one of the initial key factors that causes the obvious variance in bone formation process between our *in vivo* and *ex vivo* models is the deviation in vascularization process in the tissue-based organoid models. Numerous studies have depicted that vascularization is critical for tissue growth and development in organoid models, without which the physical diffusion of medium is not enough to provide sufficient nutrients to cells within and support their growth and development [100–102]. The vascular structures formation that grows into the macroporous scaffolds is crucial, as it brings necessary nutrients, peripheral stem cells, amino acids and protein signals that enable the tissue to grow properly [103].

The main problem is not the models being utilized, rather that we are still trying to perform bone reformation based upon an outdated knowledge subset that does not fully describe the temporal or spatial signaling cascade that occurs during bone formation. Overlooking one component's design feature will lead to misbehaving replica [72], Taken into the context of the bone formation by induction versus autogenous bone grafting, the problem remains evidently complex and multi-faceted, where there are many possible solutions [17,72].

Indeed, whilst angiogenesis is a critical aspect, a far more important paradigm is the involvement of the immunological response in light of new bone formation [104]. All bone reformation responses are based upon the host's immune system responding to a foreign invading system [4,46,78,105,106]. When biomaterials are implanted, bleeding caused by trauma introduces peripheral blood mononuclear cells (PBMCs) [107] and different cytokines into the muscle-biomaterial complex, triggering a host inflammatory response with local tissue inflammation [105,106,108] that subsequently fosters initiating the tissue repair program. Yet, when the muscle-biomaterial complex is dissected from the host environment with the disconnection of blood supply, the tissue repair process is impeded and the system loses the consistent support of the recruited PBMCs and critical cytokines, leading to a compromised immunogenic response that is needed to get good osteogenic results. The basic cell culture process thus destroys the *in vivo* impetus even to start proper tissue formation and is at best, from the present results, a weak signal that creeps along retarded because correct signals are absent [76,109]. Therefore, regardless of what organoid model is considered, proper tissue reformation is absent over a reaction that may be indicative of the actual tissue formation response. Indeed, we believe that if one could introduce PBMCs or extra cytokines such as VEGFA, BMP-2 and RANKL (for osteoclast), additional cells such as monocytes and even fresh migrating "peripheral" stem cells in a proper temporal manner to our muscle based organoid model, similarly as was witnessed partially during the *in vivo* heterotopic implantation model, it may provide the solution to generating *ex vivo* bone formation.

In conclusion, the *ex vivo* muscle pouch-based coral-derived macroporous construct organoid model has a strong potential of vascularization by means of biomimicry and replicating the tissue morphogenesis in heterotopic implantation model. However, further modification of the model, including the introduction of essential cells, signals, nutrients and improvement of direct perfusion of the vascular matrix of tissue will be required to achieve proper bone formation *ex vivo*.

Author contributions

JB performed the experiments, analyzed the data and constructed the layout and initial draft of the manuscript. CZ revised the manuscript and was instrumental in providing key ideas that lead to the data interpretation. GL conducted the additional experiments and analyzed the data. YW revised the manuscript and provided administrative support. YD revised the manuscript and supervised JB. RMK designed the project, received target agreement for materials with Zimmer Biomet, constructed discussion and methodology, revised and edited the manuscript. TH helped conceive parts of the study, interpreted the data, revised the manuscript and co-supervised JB. All authors read and approved the final manuscript.

Funding

The research was supported by the National Key Research and Development Program of China (2023YFC2812003), the Fundamental Research Funds for the Central Universities, China (YG2025QNB20), and the National Natural Science Foundation of China (82102618, 82002328).

Declaration of competing interest

The authors declare no conflict of interest.

Acknowledgement

We would like to thank M. Ponticiello and Zimmer Biomet for having provided the 13 % HA/CC coral derived scaffolds free of charge as part of the transfer agreement with Dr. Klar. We would also thank all our friends and colleagues for their help and support during the challenging periods of this project.

Appendix A. Supplementary data

Supplementary data to this article can be found online at https://doi.org/10.1016/j.jot.2025.04.002.

References

[1] Huggins CB. The formation of bone under the influence of epithelium of the urinary tract. Arch Surg 1931;22(3):377–408.
[2] Levander G. A study of bone regeneration surgery. Surg Gynecol Obstet 1938;67:705–12.
[3] Lacroix P. Recent investigations on the growth of bone. Nature 1945;156(3967).576-76.
[4] Urist MR. Bone: formation by autoinduction. Science 1965;150(3698):893–9.
[5] Sampath TK, Reddi AH. Dissociative extraction and reconstitution of extracellular matrix components involved in local bone differentiation. Proc Natl Acad Sci U S A 1981;78(12):7599–603.
[6] Wang EA, Rosen V, D'Alessandro JS, Bauduy M, Cordes P, Harada T, et al. Recombinant human bone morphogenetic protein induces bone formation. Proc Natl Acad Sci U S A 1990;87(6):2220–4.
[7] Ripamonti U. The morphogenesis of bone in replicas of porous hydroxyapatite obtained from conversion of calcium carbonate exoskeletons of coral. J Bone Joint Surg Am 1991;73(5):692–703.
[8] Reddi AH. Symbiosis of biotechnology and biomaterials: applications in tissue engineering of bone and cartilage. J Cell Biochem 1994;56(2):192–5.
[9] Ripamonti U, Duneas N, Van Den Heever B, Bosch C, Crooks J. Recombinant transforming growth factor-beta1 induces endochondral bone in the baboon and synergizes with recombinant osteogenic protein-1 (bone morphogenetic protein-7) to initiate rapid bone formation. J Bone Miner Res 1997;12(10):1584–95.
[10] Reddi AH. Morphogenesis and tissue engineering of bone and cartilage: inductive signals, stem cells, and biomimetic biomaterials. Tissue Eng 2000;6(4):351–9.
[11] Ripamonti U, Crooks J, Matsaba T, Tasker J. Induction of endochondral bone formation by recombinant human transforming growth factor-beta2 in the baboon (Papio ursinus). Growth Factors 2000;17(4):269–85.
[12] Ripamonti U, Nathaniel Ramoshebi L, Teare J, Renton L, Ferretti C. The induction of endochondral bone formation by transforming growth factor-β3: experimental studies in the non-human primate Papio ursinus. J Cell Mol Med 2008;12(3):1029–48.
[13] Klar RM, Duarte R, Dix-Peek T, Ripamonti U. The induction of bone formation by the recombinant human transforming growth factor-beta3. Biomaterials 2014;35(9):2773–88.
[14] Ripamonti U, Klar RM, Parak R, Dickens C, Dix-Peek T, Duarte R. Tissue segregation restores the induction of bone formation by the mammalian transforming growth factor-β(3) in calvarial defects of the non-human primate Papio ursinus. Biomaterials 2016;86:21–32.
[15] Pina S, Oliveira JM, Reis RL. Natural-based nanocomposites for bone tissue engineering and regenerative medicine: a review. Adv Mater 2015;27(7):1143–69.
[16] Geris L, Papantoniou I. The third era of tissue engineering: reversing the innovation drivers. Tissue Eng Part A 2019;25(11–12):821–6.
[17] Maia FR, Bastos AR, Oliveira JM, Correlo VM, Reis RL. Recent approaches towards bone tissue engineering. Bone 2022;154:116256.
[18] Herberg S, McDermott AM, Dang PN, Alt DS, Tang R, Dawahare JH, et al. Combinatorial morphogenetic and mechanical cues to mimic bone development for defect repair. Sci Adv 2019;5(8):eaax2476.
[19] Ripamonti U, Reddi AH. Geometric induction of bone formation. 1st ed. Boca Raton: CRC Press; 2021.
[20] Liu X, Li L, Gaihre B, Park S, Li Y, Terzic A, et al. Scaffold-free spheroids with two-dimensional heteronano-layers (2DHNL) enabling stem cell and osteogenic factor codelivery for bone repair. ACS Nano 2022;16(2):2741–55.
[21] Tao SC, Li XR, Wei WJ, Wei ZY, Zhang CR, Wang F, et al. Polymeric coating on beta-TCP scaffolds provides immobilization of small extracellular vesicles with surface-functionalization and ZEB1-Loading for bone defect repair in diabetes mellitus. Biomaterials 2022;283:121465.
[22] Jong-Woo Choi Y-CK. Asian facial recontouring surgery. Plastic and Aesthetic Research 2023;10(0):59.
[23] Urist MR, Strates BS. Bone morphogenetic protein. J Dent Res 1971;50(6):1392–406.
[24] Butler DL, Goldstein SA, Guilak F. Functional tissue engineering: the role of biomechanics. J Biomech Eng 2000;122(6):570–5.
[25] Tsimbouri PM, Childs PG, Pemberton GD, Yang J, Jayawarna V, Orapiriyakul W, et al. Stimulation of 3D osteogenesis by mesenchymal stem cells using a nanovibrational bioreactor. Nat Biomed Eng 2017;1(9):758–70.
[26] Hofer M, Lutolf MP. Engineering organoids. Nat Rev Mater 2021;6(5):402–20.
[27] Wang S, Wang X, Tan Z, Su Y, Liu J, Chang M, et al. Human ESC-derived expandable hepatic organoids enable therapeutic liver repopulation and pathophysiological modeling of alcoholic liver injury. Cell Res 2019;29(12):1009–26.
[28] Salahudeen AA, Choi SS, Rustagi A, Zhu J, van Unen V, dela OS, et al. Progenitor identification and SARS-CoV-2 infection in human distal lung organoids. Nature 2020;588(7839):670–5.
[29] Qu M, Xiong L, Lyu Y, Zhang X, Shen J, Guan J, et al. Establishment of intestinal organoid cultures modeling injury-associated epithelial regeneration. Cell Res 2021;31(3):259–71.
[30] Mendes LF, Katagiri H, Tam WL, Chai YC, Geris L, Roberts SJ, et al. Advancing osteochondral tissue engineering: bone morphogenetic protein, transforming growth factor, and fibroblast growth factor signaling drive ordered differentiation of periosteal cells resulting in stable cartilage and bone formation in vivo. Stem Cell Res Ther 2018;9(1):42.
[31] Kong D, Lin G, Shi Y, Gu Z, Gao Y, Feng Y. Performance of heterotopic bone elicited with bone morphogenic protein-2 microspheres as a bone repair material. Mater Des 2020;191:108657.
[32] Tan S, Wang Y, Du Y, Xiao Y, Zhang S. Injectable bone cement with magnesium-containing microspheres enhances osteogenesis via anti-inflammatory immunoregulation. Bioact Mater 2021;6(10):3411–23.
[33] Miao C, Zhou L, Tian L, Zhang Y, Zhang W, Yang F, et al. Osteogenic differentiation capacity of in vitro cultured human skeletal muscle for expedited bone tissue engineering. BioMed Res Int 2017;2017:8619385.
[34] Capel AJ, Rimington RP, Fleming JW, Player DJ, Baker LA, Turner MC, et al. Scalable 3D printed molds for human tissue engineered skeletal muscle. Front Bioeng Biotechnol 2019;7:20.
[35] Ren B, Betz VM, Thirion C, Salomon M, Jansson V, Müller PE, et al. Osteoinduction within BMP-2 transduced muscle tissue fragments with and without a fascia layer: implications for bone tissue engineering. Gene Ther 2019;26(1–2):16–28.
[36] De La Vega RE, De Padilla CL, Trujillo M, Quirk N, Porter RM, Evans CH, et al. Contribution of implanted, genetically modified muscle progenitor cells expressing BMP-2 to new bone formation in a rat osseous defect. Mol Ther 2018;26(1):208–18.
[37] He T, Hausdorf J, Chevalier Y, Klar RM. Trauma induced tissue survival in vitro with a muscle-biomaterial based osteogenic organoid system: a proof of concept study. BMC Biotechnol 2020;20(1):8.
[38] Mastrogiacomo M, Scaglione S, Martinetti R, Dolcini L, Beltrame F, Cancedda R, et al. Role of scaffold internal structure on in vivo bone formation in macroporous calcium phosphate bioceramics. Biomaterials 2006;27(17):3230–7.
[39] Koons GL, Diba M, Mikos AG. Materials design for bone-tissue engineering. Nat Rev Mater 2020;5(8):584–603.
[40] Xu Y, Saiding Q, Zhou X, Wang J, Cui W, Chen X. Electrospun fiber-based immune engineering in regenerative medicine. Smart Med 2024;3(1):e20230034.
[41] Lei Y, Zhang Q, Kuang G, Wang X, Fan Q, Ye F. Functional biomaterials for osteoarthritis treatment: from research to application. Smart Med 2022;1(1):e20220014.
[42] Weber JN, White EW, Lebiedzik J. New porous biomaterials by replication of echinoderm skeletal microstructures. Nature 1971;233(5318):337–9.

[43] Chiroff RT, White EW, Weber KN, Roy DM. Tissue ingrowth of Replamineform implants. J Biomed Mater Res 1975;9(4):29–45.
[44] White EW, Weber JN, Roy DM, Owen EL, Chiroff RT, White RA. Replamineform porous biomaterials for hard tissue implant applications. J Biomed Mater Res 1975;9(4):23–7.
[45] Ripamonti U, Crooks J, Khoali L, Roden L. The induction of bone formation by coral-derived calcium carbonate/hydroxyapatite constructs. Biomaterials 2009;30(7):1428–39.
[46] Klar RM, Duarte R, Dix-Peek T, Dickens C, Ferretti C, Ripamonti U. Calcium ions and osteoclastogenesis initiate the induction of bone formation by coral-derived macroporous constructs. J Cell Mol Med 2013;17(11):1444–57.
[47] Roy DM, Linnehan SK. Hydroxyapatite formed from coral skeletal carbonate by hydrothermal exchange. Nature 1974;247(5438):220–2.
[48] Shors EC. Coralline bone graft substitutes. Orthop Clin N Am 1999;30(4):599–613.
[49] Rowe RG, Mandelbaum J, Zon LI, Daley GQ. Engineering hematopoietic stem cells: lessons from development. Cell Stem Cell 2016;18(6):707–20.
[50] Zhang M, Shi J, Xie M, Wen J, Niibe K, Zhang X, et al. Recapitulation of cartilage/bone formation using iPSCs via biomimetic 3D rotary culture approach for developmental engineering. Biomaterials 2020;260:120334.
[51] Papantoniou I, Nilsson Hall G, Loverdou N, Lesage R, Herpelinck T, Mendes L, et al. Turning Nature's own processes into design strategies for living bone implant biomanufacturing: a decade of Developmental Engineering. Adv Drug Deliv Rev 2021;169:22–39.
[52] Lenas P, Moos M, Luyten FP. Developmental engineering: a new paradigm for the design and manufacturing of cell-based products. Part I: from three-dimensional cell growth to biomimetics of in vivo development. Tissue Eng Part B Rev 2009;15(4):381–94.
[53] Lenas P, Moos M, Luyten FP. Developmental engineering: a new paradigm for the design and manufacturing of cell-based products. Part II: from genes to networks: tissue engineering from the viewpoint of systems biology and network science. Tissue Eng Part B Rev 2009;15(4):395–422.
[54] Martin I. Engineered tissues as customized organ germs. Tissue Eng Part A 2014;20(7–8):1132–3.
[55] Freeman FE, McNamara LM. Endochondral priming: a developmental engineering strategy for bone tissue regeneration. Tissue Eng Part B Rev 2017;23(2):128–41.
[56] Marcucio RS, Qin L, Alsberg E, Boerckel JD. Reverse engineering development: crosstalk opportunities between developmental biology and tissue engineering. J Orthop Res 2017;35(11):2356–68.
[57] Urist MR, Silverman BF, Buring K, Dubuc FL, Rosenberg JM. The bone induction principle. Clin Orthop Relat Res 1967;53:243–83.
[58] Huggins CB. The formation of bone under the influence of epithelium of the urinary tract. Clin Orthop Relat Res 1968;59:7–19.
[59] Wang Z, Sun J, Li Y, Chen C, Xu Y, Zang X, et al. Experimental study of the synergistic effect and network regulation mechanisms of an applied combination of BMP-2, VEGF, and TGF-beta1 on osteogenic differentiation. J Cell Biochem 2020;121(3):2394–405.
[60] Xiong F, Cheng X, Zhang C, Klar RM, He T. Optimizations for identifying reference genes in bone and cartilage bioengineering. BMC Biotechnol 2021;21(1):25.
[61] He T, Cao C, Xu Z, Li G, Cao H, Liu X, et al. A comparison of micro-CT and histomorphometry for evaluation of osseointegration of PEO-coated titanium implants in a rat model. Sci Rep 2017;7(1):16270.
[62] Feldman AT, Wolfe D. Tissue processing and hematoxylin and eosin staining. Methods Mol Biol 2014;1180:31–43.
[63] Gruber HE. Adaptations of Goldner's Masson trichrome stain for the study of undecalcified plastic embedded bone. Biotech Histochem 1992;67(1):30–4.
[64] Bancroft JD, Bancroft JD, Gamble M. Theory and practice of histological techniques. 6th ed. Edinburgh: Churchill Livingstone; 2007.
[65] Aristotle Lanza D, Vegetti M. Opere biologiche. Torino ,: unione tipografico-editrice torinese. 1971.
[66] Shehata M. The father of medicine: a historical reconsideration. J Med Ethics 2004;12:171–6.
[67] Geuder MF, Havers Cd. Osteologia nova sive novæ quædam observationes de ossibus et partibus ad illa, pertinentibus. idiomate Anglico Londini editae. Francofurti & Lipsiæ: G.W. Kuhn; 2025.
[68] Ollier LS. Traité expérimental et clinique de la régénération des os et de la production artificielle du tissu osseux. vol. 1867; Paris, France.
[69] Senn on the healing of aseptic bone cavities by implantation of antiseptic decalcified bone. Ann Surg 1889;10(5):352–68.
[70] Autelitano L, Meazzini MC. Alveolar cleft reconstruction with vomerine bone: two surgical procedures in one step: a case series. Plastic and Aesthetic Research 2023;10(0):16.
[71] Ripamonti U. Osteoinduction in porous hydroxyapatite implanted in heterotopic sites of different animal models. Biomaterials 1996;17(1):31–5.
[72] Klar RM. The induction of bone formation: the translation enigma. Front Bioeng Biotechnol 2018;6:74.
[73] Nilsson Hall G, Mendes LF, Gklava C, Geris L, Luyten FP, Papantoniou I. Developmentally engineered callus organoid bioassemblies exhibit predictive in vivo long bone healing. Adv Sci (Weinh) 2020;7(2):1902295.
[74] Kawakami T, Kawai T, Takei N, Kise T, Eda S, Urist MR. Evaluation of heterotopic bone formation induced by squalane and bone morphogenetic protein composite. Clin Orthop Relat Res 1997;337:261–6.
[75] Ripamonti U, Ferretti C, Heliotis M. Soluble and insoluble signals and the induction of bone formation: molecular therapeutics recapitulating development. J Anat 2006;209(4):447–68.
[76] Lee E, Ko JY, Kim J, Park JW, Lee S, Im GI. Osteogenesis and angiogenesis are simultaneously enhanced in BMP2-/VEGF-transfected adipose stem cells through activation of the YAP/TAZ signaling pathway. Biomater Sci 2019;7(11):4588–602.
[77] Ripamonti U. Soluble osteogenic molecular signals and the induction of bone formation. Biomaterials 2006;27(6):807–22.
[78] Ripamonti U, Klar RM, Renton LF, Ferretti C. Synergistic induction of bone formation by hOP-1, hTGF-beta3 and inhibition by zoledronate in macroporous coral-derived hydroxyapatites. Biomaterials 2010;31(25):6400–10.
[79] Lee JH, Lee KM, Baek HR, Jang SJ, Lee JH, Ryu HS. Combined effects of porous hydroxyapatite and demineralized bone matrix on bone induction: in vitro and in vivo study using a nude rat model. Biomed Mater 2011;6(1):015008.
[80] Zhou K, Yu P, Shi X, Ling T, Zeng W, Chen A, et al. Hierarchically porous hydroxyapatite hybrid scaffold incorporated with reduced graphene oxide for rapid bone ingrowth and repair. ACS Nano 2019;13(8):9595–606.
[81] Fricain JC, Schlaubitz S, Le Visage C, Arnault I, Derkaoui SM, Siadous R, et al. A nano-hydroxyapatite–pullulan/dextran polysaccharide composite macroporous material for bone tissue engineering. Biomaterials 2013;34(12):2947–59.
[82] Swanson WB, Omi M, Zhang Z, Nam HK, Jung Y, Wang G, et al. Macropore design of tissue engineering scaffolds regulates mesenchymal stem cell differentiation fate. Biomaterials 2021;272:120769.
[83] Fitzpatrick V, Martin-Moldes Z, Deck A, Torres-Sanchez R, Valat A, Cairns D, et al. Functionalized 3D-printed silk-hydroxyapatite scaffolds for enhanced bone regeneration with innervation and vascularization. Biomaterials 2021;276:120995.
[84] Du B, Liu W, Deng Y, Li S, Liu X, Gao Y, et al. Angiogenesis and bone regeneration of porous nano-hydroxyapatite/coralline blocks coated with rhVEGF165 in critical-size alveolar bone defects in vivo. Int J Nanomed 2015;10:2555–65.
[85] Zhang H, Zhou Y, Yu N, Ma H, Wang K, Liu J, et al. Construction of vascularized tissue-engineered bone with polylysine-modified coral hydroxyapatite and a double cell-sheet complex to repair a large radius bone defect in rabbits. Acta Biomater 2019;91:82–98.
[86] Asatrian G, Chang L, James AW. Muscle pouch implantation: an ectopic bone formation model. Methods Mol Biol 2014;1213:185–91.
[87] Scotti C, Piccinini E, Takizawa H, Todorov A, Bourgine P, Papadimitropoulos A, et al. Engineering of a functional bone organ through endochondral ossification. Proc Natl Acad Sci U S A 2013;110(10):3997–4002.
[88] Lee J, Lee S, Ahmad T, Madhurakkat Perikamana SK, Lee J, Kim EM, et al. Human adipose-derived stem cell spheroids incorporating platelet-derived growth factor (PDGF) and bio-minerals for vascularized bone tissue engineering. Biomaterials 2020;255:120192.
[89] Trueta J, Buhr AJ. The vascular contribution to osteogenesis. V. The vasculature supplying the Epiphysial cartilage in Rachitic rats. J Bone Joint Surg Br 1963;45:572–81.
[90] Shahabipour F, Ashammakhi N, Oskuee RK, Bonakdar S, Hoffman T, Shokrgozar MA, et al. Key components of engineering vascularized 3-dimensional bioprinted bone constructs. Transl Res 2020;216:57–76.
[91] Wenyu Xia WW, Qin Yi, Ding Yayun, Li Wenhao, Ge Gaoran, Li Wenming, et al. Crosstalk between bone and vasculature within bone. Fundamental Research 2025:S266732582500007X.
[92] Homan KA, Gupta N, Kroll KT, Kolesky DB, Skylar-Scott M, Miyoshi T, et al. Flow-enhanced vascularization and maturation of kidney organoids in vitro. Nat Methods 2019;16(3):255–62.
[93] Bai Y, Bai L, Zhou J, Chen H, Zhang L. Sequential delivery of VEGF, FGF-2 and PDGF from the polymeric system enhance HUVECs angiogenesis in vitro and CAM angiogenesis. Cell Immunol 2018;323:19–32.
[94] Jain RK. Molecular regulation of vessel maturation. Nat Med 2003;9(6):685–93.
[95] Gould DB, Phalan FC, van Mil SE, Sundberg JP, Vahedi K, Massin P, et al. Role of COL4A1 in small-vessel disease and hemorrhagic stroke. N Engl J Med 2006;354(14):1489–96.
[96] Risau W. Mechanisms of angiogenesis. Nature 1997;386(6626):671–4.
[97] Javed A, Chen H, Ghori FY. Genetic and transcriptional control of bone formation. Oral Maxillofac Surg Clin North Am 2010;22(3):283–93.
[98] Gerber HP, Vu TH, Ryan AM, Kowalski J, Werb Z, Ferrara N. VEGF couples hypertrophic cartilage remodeling, ossification and angiogenesis during endochondral bone formation. Nat Med 1999;5(6):623–8.
[99] Xiao G, Jiang D, Ge C, Zhao Z, Lai Y, Boules H, et al. Cooperative interactions between activating transcription factor 4 and Runx2/Cbfa1 stimulate osteoblast-specific osteocalcin gene expression. J Biol Chem 2005;280(35):30689–96.
[100] Sharma D, Ross D, Wang G, Jia W, Kirkpatrick SJ, Zhao F. Upgrading prevascularization in tissue engineering: a review of strategies for promoting highly organized microvascular network formation. Acta Biomater 2019;95:112–30.
[101] Vargas-Valderrama A, Messina A, Mitjavila-Garcia MT, Guenou H. The endothelium, a key actor in organ development and hPSC-derived organoid vascularization. J Biomed Sci 2020;27(1):67.
[102] Zhang S, Wan Z, Kamm RD. Vascularized organoids on a chip: strategies for engineering organoids with functional vasculature. Lab Chip 2021;21(3):473–88.
[103] Filipowska J, Tomaszewski KA, Niedzwiedzki L, Walocha JA, Niedzwiedzki T. The role of vasculature in bone development, regeneration and proper systemic functioning. Angiogenesis 2017;20(3):291–302.
[104] Vishwakarma A, Bhise NS, Evangelista MB, Rouwkema J, Dokmeci MR, Ghaemmaghami AM, et al. Engineering immunomodulatory biomaterials to tune the inflammatory response. Trends Biotechnol 2016;34(6):470–82.

[105] Trindade R, Albrektsson T, Tengvall P, Wennerberg A. Foreign body reaction to biomaterials: on mechanisms for buildup and breakdown of osseointegration. Clin Implant Dent Relat Res 2016;18(1):192–203.
[106] Sheikh Z, Hamdan N, Ikeda Y, Grynpas M, Ganss B, Glogauer M. Natural graft tissues and synthetic biomaterials for periodontal and alveolar bone reconstructive applications: a review. Biomater Res 2017;21:9.
[107] Rüger BM, Buchacher T, Dauber E-M, Pasztorek M, Uhrin P, Fischer MB, et al. De novo vessel formation through cross-talk of blood-derived cells and mesenchymal stromal cells in the absence of pre-existing vascular structures. Front Bioeng Biotechnol 2020;8.
[108] Zhou G, Groth T. Host responses to biomaterials and anti-inflammatory design-a brief review. Macromol Biosci 2018;18(8):e1800112.
[109] Chen YC, Lin RZ, Qi H, Yang Y, Bae H, Melero-Martin JM, et al. Functional human vascular network generated in photocrosslinkable gelatin methacrylate hydrogels. Adv Funct Mater 2012;22(10):2027–39.